CRITICAL HEAT FLUX IN POOL BOILING ON METAL-GRAPHITE COMPOSITE SURFACES

Nengli Zhang
Ohio Aerospace Institute/NASA Glenn Research Center, Cleveland, OH 44135

Wen-Jei Yang
Department of Mechanical Engineering and Applied
Mechanics, University of Michigan, Ann Arbor, Michigan 48109-2125, USA

David F. Chao
NASA Glenn Research Center, Cleveland, OH 44135

ABSTRACT

A study is conducted on high heat-flux pool boiling of pentane on micro-configured composite surfaces. The boiling surfaces are copper-graphite (Cu-Gr) and aluminum-graphite (Al-Gr) composites with a fiber volume concentration of 50%. The micro-graphite fibers embedded in the matrix contribute to a substantial enhancement in boiling heat-transfer performance. Correlation equations are obtained for both the isolated and coalesced bubble regimes, utilizing a mathematical model based on a metal-graphite, two-tier configuration with the aid of experimental data. A new model to predict the critical heat flux (CHF) on the composites is proposed to explain the fundamental aspects of the boiling phenomena. Three different factors affecting the CHF are considered in the model. Two of them are expected to become the main agents driving vapor volume detachment under microgravity conditions, using the metal-graphite composite surfaces as the heating surface and using liquids with an unusual Marangoni effect as the working fluid.

NOMENCLATURE

C_1	constant defined by Eq. (6)
C_s	constant (J/s cm^2 $^\circ$C^m)
d	fiber diameter (m)
D	micro bubble diameter (m)
f	frequency of micro bubbles (1/s)
g	acceleration due to gravity (m/s^2)
h_{fg}	latent heat of vaporization at boiling point (J/kg)
k	thermal conductivity (W/m K)
m	constant
n	active site density (1/cm^2)
n_t	number of graphite fiber tips in a vapor column
N	density of vapor stem (1/cm^2)
q	heat flux (W/cm^2)
T	temperature ($^\circ$C)
ΔT_i	temperature difference between heating wall surface and interface along macrolayer ($^\circ$C)
ΔT_t	superheat at transition from isolated to coalesced bubble regime ($^\circ$C)
ΔT_{sat}	superheat ($^\circ$C)
ΔT_{wb}	temperature difference between heating wall surface and bulk liquid
U_{vc}	critical velocity of vapor jet (m/s)
V_l	liquid volume entrapped between bubbles (cm^3)

Greek Symbols

α	area fraction of fibers in base material
δ	macrolayer thickness (m)

η	constant
λ_c	Helmholtz-unstable wavelength (m)
λ_d	Taylor wave node spacing (m)
θ	contact angle (deg.)
ρ	density (kg/m^3)
σ	surface tension (N/m)
$\Delta\psi$	available energy (N m)
ζ	constant

Subscripts
C	critical
g	due to gravity
h	high heat flux region
i	interface along macrolayer
l	low heat flux region or liquid
m	maximum
sat	saturation
t	transition
v	saturated vapor
w	wall
σ	due to surface tension
$\Delta\sigma$	due to surface-tension gradient
Zuber	given by Zuber model

INTRODUCTION

Nucleate boiling near the critical heat flux (CHF) can provide excellent economy along with high efficiency of heat transfer. However, nucleate boiling performance may deteriorate in a reduced gravity environment and nucleate boiling usually has a potentially dangerous characteristic in the CHF regime. That is, any slight overload can result in burnout of the boiling surface because the heat transfer will suddenly move into the film-boiling regime. Webb [1] and Thome [2, 3] provided general reviews of boiling enhancement surfaces. Some of the surfaces can both enhance nucleate boiling heat transfer and increase the CHF, but some only enhance the nucleate boiling without either increase or much of a decrease in the CHF value [4]. Recently, O'Connor and You [5] investigated a painting technique to create a surface microstructure for enhanced boiling heat transfer. They reported an increase in boiling heat transfer three times greater than the unpainted surface, and a CHF increase of 109 percent. They pointed out that the CHF increase was due to surface microstructure and its influence on boiling heat transfer characteristics.

The most widely accepted correlations for CHF, developed by Zuber [6] and Haramura and Katto [7], are only applicable to smooth surfaces because the correlations do not account for surface effects. Wright and Gebhart [8, 9] investigated enhanced boiling performance on micro-configured surfaces and suggested a two-bubble model to explain the enhancement of the boiling heat transfer on the surfaces. Yang et al. [10, 11] initiated an intensive study on nucleate pool boiling on micro-composite surfaces. They found that boiling heat transfer on copper-graphite composite

surfaces is higher than that on pure metal surfaces by a factor of 3 to 6. A two-tier model was proposed by Zhang et al [12] to explain the nucleate boiling process and performance enhancement on micro-configured surfaces. Yang and Zhang [13] divided composite enhanced surfaces into two categories: discrete insert/matrix-type composites and micro-configured insert-into-matrix types. They presented a hypothesis to explain the formation of the plateau of the boiling curve in the CHF region. This explanation may provide a guideline for searching for the proper construction of enhanced boiling surfaces with a wider "safety" margin in the CHF regime.

Most recently, the authors have proposed a model to predict the CHF on metal-graphite composites [14]. However, the nucleate boiling mechanisms on composite surfaces, especially in the CHF regime, have not been adequately studied.

CORRELATIONS FOR POOL NUCLEATE BOILING

Experimental studies were performed on nucleate pool boiling of pentane on cooper-graphite (Cu-Gr) and aluminum-graphite (Al-Gr) composite surfaces with various fiber volume concentrations for heat fluxes up to 35 W/cm^2. They revealed that the onset of nucleate boiling (the isolated bubble regime) occurs at wall superheat of about 10 °C for the Cu-Gr surface and 15 °C for the Al-Gr surface, with a fiber volume concentration of 50%, much lower than their respective pure metal surfaces. A significant enhancement in boiling heat-transfer performance on the composite surfaces is achieved [15], as shown in Fig.1, due to the presence of micro-graphite fibers embedded in the matrix. Transition from an isolated bubble regime to a coalesced bubble regime in boiling occurs at a superheat of about 14 °C on a Cu-Gr surface and 19 °C on an Al-Gr surface.

According to a two-tier configuration and its mathematical model [12], and based on the existing experimental data, correlations for the boiling heat-transfer performance in the isolated bubble regime and in the coalesced bubble regime are obtained as follows:

The boiling heat flux in the low heat flux boiling region (isolated bubble regime) is mainly contributed by micro bubbles, with negligible heat conduction across the microlayer, and can be expressed as

$$q_l = nf \frac{\pi D_m^3}{6} \rho_v h_{fg} \tag{1}$$

where n is the active site density, f is the frequency of micro bubbles emitted from a tip of the graphite fiber, D_m is the maximum micro bubble diameter, ρ_v is the density of saturated vapor at the boiling point, and h_{fg} is the latent heat of vaporization at the boiling point. For the composite surfaces, D_m is related to the fiber diameter, d, and the area fraction of the fibers in the base material, α, which equals fiber volume concentration, by

$$D_m = \frac{d}{2}\sqrt{\frac{\pi}{\alpha}} \qquad (2)$$

In the case of $\alpha = 0.25$ and $d = 8$ μm, the value of D_m is calculated at about 14 μm.

The generation rate of the micro bubbles from the composite surface, nf, depends on the superheat $\Delta T_{sat}=T_w-T_{sat}$, and can be given by $C_s(\Delta T_{sat})^m$, where C_s and m are constants determined by the experimental data. Then, Eq. (1) can be written as

$$q_l = \frac{\pi D_m^3}{6}\rho_v h_{fg} C_s (\Delta T_{sat})^m \qquad (3)$$

It is noted that the heat flux contributed by micro bubbles reaches maximum when the boiling comes up to the transition from the isolated bubble regime to the coalesced bubble regime where the superheat $\Delta T_t = T_{w,t} - T_{sat}$, $T_{w,t}$ is the heating wall surface temperature at the transition.

In the high heat flux boiling region (coalesced bubble regime), the boiling heat flux consists of two parts: latent heat transport by micro bubbles under the vapor stems, and by evaporation on the interface along the macrolayer, which equals heat conduction across the macrolayer. The total heat flux is

$$q_h = q_{l,m} + \frac{N V_l k_l \Delta T_i}{\delta^2} \qquad (4)$$

where $q_{l,m}$ is the heat flux contributed by micro bubbles that equals the maximum value of the heat flux in the isolated bubble regime, N is the density of the vapor stem, V_l is the liquid volume being entrapped between the bubbles, k_l is the thermal conductivity of the working fluid, $\Delta T_i=T_w-T_i$ is the temperature difference between the heating wall surface and the interface along the macrolayer, and δ is the macrolayer thickness. The temperature along the macrolayer interface in the coalesced bubble regime, T_i, can be considered approximately to equal the heating surface temperature at the transition from the isolated bubble regime to the coalesced bubble regime, $T_{w,t}$. Thus we can write Eq. (4) as

$$q_h = \frac{\pi D_m^3}{6}\rho_v h_{fg} C_s (\Delta T_i)^m + k_l C_l (\Delta T_{sat} - \Delta T_i) \qquad (5)$$

where

$$C_l = \frac{N V_l}{\delta^2} \qquad (6)$$

which is a constant and can be determined by experiments.

Based on experimental data, the values of the constants C_s, m, and C_l, were estimated at 2.828×10^7, 2.443, and 2.389×10^3, respectively for the Cu-Gr composite surface, and 2.544×10^5, 3.805, and 3.39×10^3, respectively for the Al-Gr composite surface for the cases of $\alpha = 0.5$ [17]. Figure 1 shows the experimental data and the curves that resulted from Eqs. (3) and (5).

CRITICAL HEAT FLUX

It is well known that there are two primary models to explain the fundamental mechanism of the CHF in saturated pool boiling: the hydrodynamic instability model and the macrolayer dry-out model; both models lead to the same result [18]. Applying Kelvin-Helmholtz instability and Taylor wave theories to the CHF on the metal-graphite composite surfaces, Yang and Zhang [14] proposed a model to predict the CHF on the composite surfaces. They found that in the metal-graphite cases the Helmholtz-unstable wavelength is

$$\lambda_{lc} = 2\pi\left(\frac{\sigma}{g(\rho_l - \rho_v)}\right)^{1/2} \qquad (7)$$

and the critical velocity of vapor jet is

$$U_{vc} = \left(\frac{2\pi\sigma}{\rho_v \lambda_c}\right)^{1/2} \frac{[\rho_l(\rho_l + \rho_v)]^{1/2}\left(\frac{2\sqrt{3}\alpha}{\pi}-1\right)}{\rho_v + \rho_l\left(\frac{2\sqrt{3}\alpha}{\pi}-1\right)} \qquad (8)$$

where σ is the surface tension of the liquid, and g is the gravitational acceleration. Note that the Helmholtz-unstable wavelength, λ_c, for the composite surface is only $1/\sqrt{3}$ of that for pure metal surfaces. It is interesting that the experimental results show that the boiling curves of metal-graphite composites with different graphite fiber concentrations converge near the critical heat flux [15]. This implies that all boiling curves will congregate at the critical point of a particular graphite-fiber concentration $\alpha_c=1/4$ which yields the optimum nucleate boiling performance. Thus, Eq. (8) is reduced to

$$U_{vc} = \left(\frac{2\pi\sigma}{\rho_v \lambda_c}\right)^{1/2} \frac{[\rho_l(\rho_l + \rho_v)]^{1/2}\left(\frac{\sqrt{3}/2}{\pi}-1\right)}{\rho_v + \rho_l\left(\frac{\sqrt{3}/2}{\pi}-1\right)} \qquad (9)$$

Then, the CHF is given by

$$q_C = \frac{2\pi}{\sqrt{3}}\rho_v h_{fg} U_{vc} \qquad (10)$$

It is obvious that the CHF depends on the gravity through Helmholtz-unstable wavelength, λ_c, and will largely undervalue the CHF under microgravity conditions.

The hydrodynamic model of CHF from the viewpoint of associated available energy proposed by Mcgills and Carey [21] may also be modified to incorporate the effects of the metal-graphite composite surfaces. The unique characteristics of the metal-graphite composite surfaces make it easier for the bubbles to detach from them than from pure-metal surfaces. Due to the poor wetting characteristics of graphite, each new micro bubble has a continually extending base and also a larger surface-tension force that helps to keep it attached to the tip. As the new bubbles on the fiber tips grow, they attract micro bubbles residing in the valleys between the fiber tips. Hence, the bubbles sit on the tips instead of within the valleys in the high heat flux regime, with a neck near the tip surface for its large contact angle, $\theta > 90°$, as shown in Figs. 2(a) to (c). The vapor columns formed at CHF have the same character, with a neck at the foot, as shown in Fig. 2(d). The surface tension facilitates the vapor volume detachment through a necking process near the composite surface. Thus, in the hydrodynamic instability analysis of the vapor columns for the CHF, following a method similar to that of McGillis and Carey [21], the available energy of surface tension

$$\Delta \psi_\sigma = -\eta n_t \sigma \pi d \cos\theta \frac{d}{2} \tag{11}$$

should be added to the total available energy. Where, η is a correction factor, and n_t is the number of the graphite fiber tips where the vapor sat on in the vapor column. Substituting the $n_t = (\alpha/4)(\lambda_d/d)^2$ into the Eq. (11), we write $\Delta \psi_\sigma$ as

$$\Delta \psi_\sigma = -\eta \alpha \sigma \frac{\pi \lambda_d^2}{8} \cos\theta \tag{12}$$

where λ_d is the Taylor wave node spacing defined as $2\pi[3\sigma/(\rho_l-\rho_v)g]^{1/2}$. Additionally, as analyzed by Zhang et al. [22, 17], the available energy associated with the Marangoni flow driven by surface-tension gradient

$$\Delta \psi_{\Delta\sigma} = \zeta \frac{\partial \sigma}{\partial T} \Delta T_{wb} (\pi \frac{\lambda_d}{2}) \lambda_d \tag{13}$$

should be also counted in the total available energy. Therefore, the total available energy is

$$\Delta \psi = \frac{\pi}{32}(\rho_l - \rho_v)\lambda_d^4 g + \zeta \frac{\pi}{2} \frac{\partial \sigma}{\partial T} \Delta T_{wb} \lambda_d^2 - \eta \alpha \sigma \pi \cos\theta \frac{\lambda_d^2}{8} \tag{14}$$

where z is the correction factor, and ΔT_{wb} is the temperature difference between the heating surface and the bulk liquid. As pointed out by Zhang et al., the second term of the right side of Eq. (14) is unfavorable to the CHF when normal pure liquids are used as the working fluid -- they have negative surface tension gradients with temperature. Usually, this can be ignored in pure liquids because of the small value of the

surface tension gradient on the liquid-vapor interface. However, when dilute aqueous solutions of long-chain alcohols, which have an unusual Marangoni effect, are used as the working fluid, this term becomes a considerably larger positive value, and therefore enhances the CHF. According to Zuber's model [21], the CHF is given by

$$q_{C,Zuber} = \frac{\pi}{24} \rho_v h_{fg} \left(\frac{32\sigma\Delta\psi_g}{\pi\lambda_d^4\rho_v^2} \right)^{1/4} \tag{15}$$

where $\Delta\psi_g$ is the available gravitational energy that equals the first term of the right side of Eq. (14). Replacement of $\Delta\psi_g$ by $\Delta\psi$ in Eq. (15) yields

$$q_C = q_{C,Zuber} \left(1 + \frac{4}{3\pi^2\sigma} \zeta \frac{\partial \sigma}{\partial T} \Delta T_{wb} - \frac{\eta\alpha\cos\theta}{3\pi^2} \right)^{1/4} \tag{16}$$

Based on the experimental results, all boiling curves will congregate at the critical point of a particular graphite-fiber concentration $\alpha_c = 1/4$ as mentioned above, and therefore for the metal-graphite composite surface the CHF is given by

$$q_C = q_{C,Zuber} \left(1 + \frac{4}{3\pi^2\sigma} \zeta \frac{\partial \sigma}{\partial T} \Delta T_{wb} - \frac{\eta\cos\theta}{12\pi^2} \right)^{1/4} \tag{17}$$

DISCUSSION

The enhancement mechanism of the boiling on the composite surfaces is due to the facilitation of the necking process of bubbles on the graphite tips. It is well known that for conventional pure metal heating surfaces the surface tension drags the bubbles to resist departure. However, for the metal-graphite composite surfaces the bubbles form a neck just above their foot and the surface tension at the neck promotes the departure of the bubbles through the necking process. This unique necking character of the composite surfaces also promotes the detachment of mushroom-shape bubbles in the high heat flux regime and the vapor columns at the CHF region. The effect of this character is reflected in the third term in the bracket of the right side of Eq. (17).

The first term in the bracket of the right side of Eq. (17) reflects the gravity role, which is the main agent of bubble detachment on the earth, and may masks other agents. The second term is the effect of the propulsive force produced by Marangoni flow around the vapor volumes. For pure working fluids, which have a negative surface tension-temperature gradient, the propulsive force tends to keep the vapor volumes pressed to the heating surface.

It is suggested that the combination of applying the liquids with positive surface tension gradient with temperature as the working fluid, and using the metal-graphite composite materials as the heating surface, will greatly enhance boiling heat transfer. Both are independent of gravity, and therefore,

4

will become main agents driving vapor volume detachment from heat surfaces and enhancing the CHF of boiling heat transfer under microgravity conditions.

CONCLUSIONS

Metal-graphite composite surfaces not only enhance the boiling heat transfer in nucleate boiling regimes but also at the CHF. The mechanism of the enhancements is analyzed and a new model is proposed to predict the CHF on composite surfaces. Three different factors affecting the CHF are considered in the model. Two of them will become the main agents driving vapor volume detachment under microgravity conditions through use of the metal-graphite composite surfaces as heating surfaces and liquids with an unusual Marangoni effect as working fluids.

REFERENCES

1. Webb, R. L., 1981, "The Evolution of Enhanced Surface Geometries for Nucleate Boiling," *Heat Transfer Engineering*, Vol. 2, No. 3-4, pp. 46-69.
2. Thome, J. R., 1990, "Enhanced Boiling Heat Transfer," Hemisphere Publishing Corp., New York, 1990.
3. Thome, J. R., 1992, "Mechanism of Enhanced Nucleate Pool Boiling," *Proceedings of Engineering Foundation Conference on Pool and External Flow Boiling, March 22 -27, 1992 / Santa Barbara, California*, pp. 337-343.
4. Yilmaz, S., and Westwater, J. W., 1981, "Effect of Commercial Enhanced Surfaces on the Boiling Heat Transfer Curve," In *Advances in Enhanced Heat Transfer, ASME, HTD Vol. 18, New York*, pp. 73-91.
5. O'Connor. J. P., and You, S. M., 1995, "A Painting Technique to Enhanced Pool Boiling Heat Transfer in Saturated FC-72," *Journal of Heat Transfer*, Vol. 117, 387-393.
6. Zuber, N., 1959, "Hydrodynamic Aspects of Boiling Heat Transfer," *AEC Report No. AECU-4439, Physics and Mathematics*.
7. Haramura, Y., and Katto, Y., 1983, "A New Hydrodynamic Model of the Critical Heat Flux, Applicable to Both Pool and Forced Convective Boiling on Submerged Bodies in Saturated Liquids," *International Journal of Heat and Mass Transfer*, Vol. 26, pp. 389-399.
8. Wright, N., and Gebhart, B., 1989, "Enhanced Boiling on Microconfigured Surfaces," *Journal of Electronic Packaging*, Vol. 111, pp. 112-120.
9. Wright, N., and Gebhart, B., 1992, "A Two Bubble Model of Boiling Enhancement from Microconfigured Surfaces," *Proceedings of Engineering Foundation Conference on Pool and External Flow Boiling, March 22 -27, 1992 / Santa Barbara, California*, pp. 367-372.
10. Yang, W. J., Takizawa, H., and Vrable, D. L., 1991, "Augmented Boiling on Copper-Graphite Composite Surface," *International Journal of Heat and Mass Transfer*, Vol. 34, No. 11, pp. 2751-2758.
11. Yang, W. J., Takizawa, H., and Vrable, D. L., 1991, "Natural Convection from a Horizontal Heated Copper-Graphite Composite Surface," *Journal of Heat Transfer*, Vol. 113, pp. 1031-1033.
12. Zhang, N., Yang, W. J., and Yang, G. W., 1992, "Two-tier Model for Nucleate Pool Boiling Heat Transfer on Microconfigured Surfaces," *International Communication Journal of Heat and Mass Transfer*, Vol. 19, No. 6, pp. 767-779.
13. Yang, W. J., and Zhang, N., 1992, "Boiling Performance on Nonisothermal Surfaces," *Proceedings of Engineering Foundation Conference on Pool and External Flow Boiling, March 22 -27, 1992 / Santa Barbara, California*, pp. 119-124.
14. Yang, W. J., and Zhang, N., 1999, "A Theoretical Treatment of Critical Heat Flux on Metal-Graphite Heating Surfaces," *Proceedings of the ASME Heat Transfer Division-1999*, HTD-Vol. 364-2, pp. 315-320.
15. Liang, H-S., 1997, "Nucleate Pool Boiling on Micro-Graphite-Fiber Composite Surfaces with Applications in Micro-Electronic Cooling," PhD. Thesis, The University of Michigan, Ann Arbor, Michigan, 1997.
16. Vargaftik, N. B., 1983, "Handbook of Physical Properties of Liquids and Gases," Hemisphere Publishing Corporation, Washington, D.C., U.S.A..
17. Zhang, N., Chao, D. F., and Yang, W. J., 2000, "Enhancements of Nucleate Boiling under Microgravity Conditions," *38th Aerospace Sciences Meeting & Exhibition, January 10-13, 2000 / Reno, NV*..
18. Katto, Y., 1992, "Critical Heat Flux in Pool Boiling," *Proceedings of Engineering Foundation Conference on Pool and External Flow Boiling, March 22 -27, 1992 / Santa Barbara, California*, pp. 151-164.
19. Liang, H. S., and Yamg, W. J., 1998, "Nucleate Pool Boiling Heat Transfer in a Highly Wetting Liquid on Micro-Graphite-Fiber Composite Surfaces," *International Journal Heat and Mass Transfer*, Vol. 41, pp. 1993-2001.
20. Yang, G. W., 1995, "Micro- and Macro-Phenomena in Nucleate Pool Boiling on Graphite-Copper Composite Materials," PhD. Thesis, The University of Michigan, Ann Arbor, Michigan, 1995.
21. McGillis, W. R., and Carey, V. P., 1996, "On the Role of Marangoni Effects on the Critical Heat Flux for Pool Boiling of Binary Mixtures," *Journal of Heat and Mass Transfer*, Vol. 118, pp. 103-118.
22. Zhang, N., and Chao, D. F., 1999, "Models for Enhanced Boiling Heat Transfer by Unusual Marangoni Effects under Microgravity Conditions," *Int. Comm. Heat Mass Transfer*, Vol. 26, pp. 1081-1090.
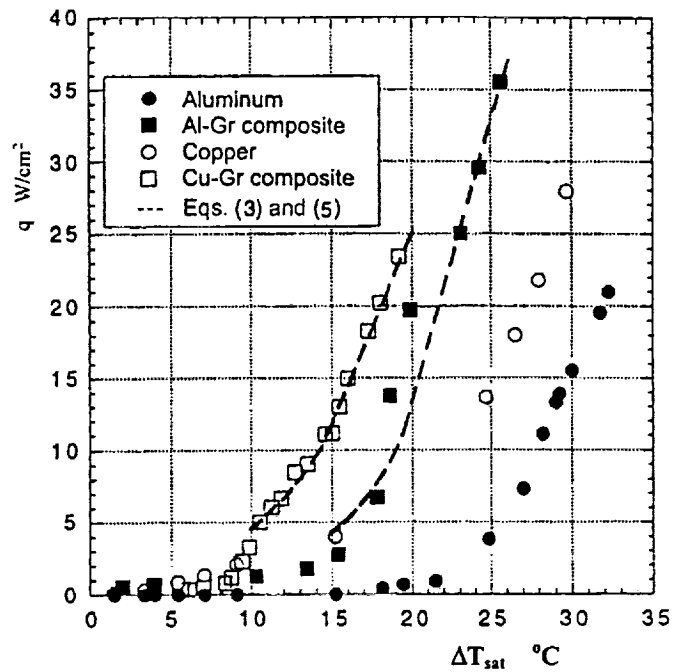
Fig. 1 Pool boiling performances of pentane on different surfaces

(a)
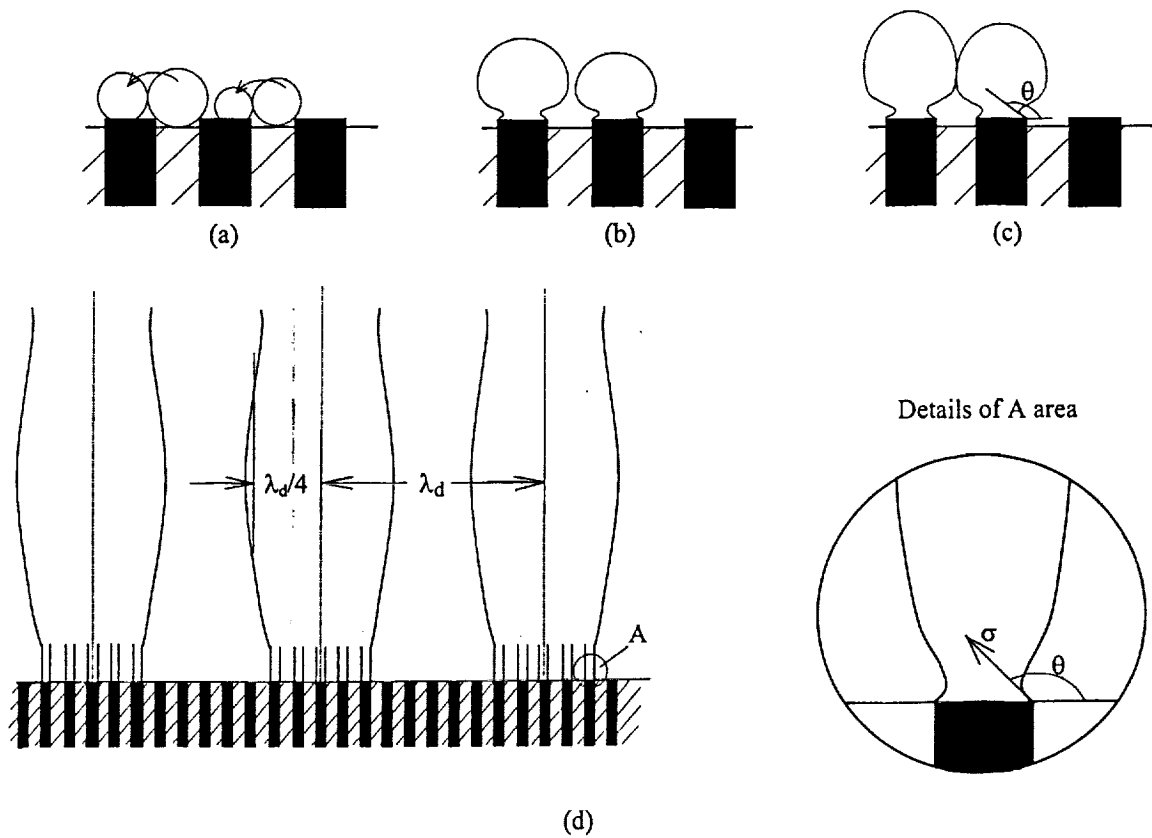
(b)

(c)

$\lambda_d/4$ λ_d

A

Details of A area

σ θ

(d)

Fig. 2 Vapor columns in CHF